doi:10.1093/jmcb/mjy043
Published online July 28, 2018

Article

Vertebrate Dynein-f depends on Wdr78 for axonemal localization and is essential for ciliary beat

Yirong Zhang†, Yawen Chen†, Jianqun Zheng, Juan Wang, Shichao Duan, Wei Zhang, Xiumin Yan*, and Xueliang Zhu*

State Key Laboratory of Cell Biology, CAS Center for Excellence in Molecular Cell Science, Shanghai Institute of Biochemistry and Cell Biology, University of Chinese Academy of Sciences, Chinese Academy of Sciences, 320 Yueyang Road, Shanghai 200031, China
† These authors contributed equally to this work.
* Correspondence to: Xueliang Zhu, E-mail: xlzhu@sibcb.ac.cn; Xiumin Yan, E-mail: yanx@sibcb.ac.cn

Edited by Xuebiao Yao

Motile cilia and flagella are microtubule-based organelles important for cell locomotion and extracellular liquid flow through beating. Although axonenal dyneins that drive ciliary beat have been extensively studied in unicellular *Chlamydomonas*, to what extent such knowledge can be applied to vertebrate is poorly known. In *Chlamydomonas*, Dynein-f controls flagellar waveforms but is dispensable for beating. The flagellar assembly of its heavy chains (HCs) requires its intermediate chain (IC) IC140 but not IC138. Here we show that, unlike its *Chlamydomonas* counterpart, vertebrate Dynein-f is essential for ciliary beat. We confirmed that Wdr78 is the vertebrate orthologue of IC138. Wdr78 associated with Dynein-f subunits such as Dnah2 (a HC) and Wdr63 (IC140 orthologue). It was expressed as a motile cilium-specific protein in mammalian cells. Depletion of Wdr78 or Dnah2 by RNAi paralyzed mouse ependymal cilia. Zebrafish *Wdr78* morphants displayed ciliopathy-related phenotypes, such as curved bodies, hydrocephalus, abnormal otolith, randomized left–right asymmetry, and pronephric cysts, accompanied with paralyzed pronephric cilia. Furthermore, all the HCs and ICs of Dynein-f failed to localize in the Wdr78-depleted mouse ependymal cilia. Therefore, both the functions and subunit dependency of Dynein-f are altered in evolution, probably to comply with ciliary roles in higher organisms.

Keywords: axonemal dynein, Dynein-f, IC138, motile cilium, primary ciliary dyskinesia, Wdr78, Dnah2

Introduction

Motile cilia or flagella are hair-like organelles protruding from the cell surface. They are evolutionarily conserved from unicellular protozoa to human. Ciliary beating propels cell locomotion and extracellular fluid flow (Fliegauf et al., 2007; Satir and Christensen, 2007). In higher animals, motile cilia are enriched in the brain ventricles, spinal canal, trachea, and reproductive organs. Dysfunction of motile cilia, usually caused by abnormalities in ciliary structure, results in primary ciliary dyskinesia (PCD) (Fliegauf et al., 2007; Brooks and Wallingford, 2014; Praveen et al., 2015). The majority of motile cilia, such as those in mammalian trachea, ependyma, and zebrafish pronephros, contain a '9 + 2' microtubule (MT) array, i.e. with nine peripheral MT doublets surrounding a central pair (CP) of MTs. Such type of cilia usually beats in a back-and-forth, or planar, fashion. A small portion, including those in zebrafish spinal cord, lacks the CP ('9 + 0') and beats in a rotational pattern (Kramer-Zucker et al., 2005; Satir and Christensen, 2007; Guirao et al., 2010; Teves et al., 2016).

Ciliary motility is driven by axonemal dyneins. Electron microscopy and cryo-electron tomography studies reveal that four homogeneous outer dynein arms (ODAs) and seven heterogeneous inner dynein arms (IDAs) are organized in a 96-nm repetitive pattern along the A-tubule of each MT doublet to face the B-tubule of the adjacent MT doublet (Nicastro et al., 2006; Mizuno et al., 2012; Viswanadha et al., 2017). As these dyneins are MT-based molecular motors possessing ATPase activities, they can convert the chemical energy of ATP into relative sliding between adjacent MT doublets to generate ciliary bending (Ishikawa, 2012; Mizuno et al., 2012; King, 2016; Viswanadha et al., 2017).

Current knowledge on the regulation of ciliary motility is mainly from studies in protozoan model organisms such as

Received March 2, 2018. Revised May 11, 2018. Accepted July 27, 2018.

Chlamydomonas reinhardtii, which contains two '9 + 2' type of motile cilia (or flagella). In *Chlamydomonas*, ODAs are required for ciliary beat frequency (CBF), whereas IDAs are responsible for bend formation and beating form (Brokaw and Kamiya, 1987; Kamiya, 2002; VanderWaal et al., 2011; King, 2012). Among these ODAs and IDAs, the inner dynein arm-f (Dynein-f, also called I1 dynein) is the best characterized. Dynein-f is the only two-headed IDA, composed of two heavy chains (HCs), 1α HC and 1β HC, three intermediate chains (ICs), IC140, IC138 and IC97, a light intermediate chain, FAP120, and several light chains (LCs), LC7a, LC7b, LC8, Tctex1, and Tctex2b. It is located at the proximal side of each 96-nm repeat near the first radial spoke (RS) (Wirschell et al., 2007; Mizuno et al., 2012; King, 2016; Viswanadha et al., 2017). In *Chlamydomonas* mutants lacking Dynein-f, flagella display normal CBF but their bending amplitudes are reduced (Myster et al., 1997, 1999).

IC138 is a key regulatory subunit of *Chlamydomonas* Dynein-f. It interacts with IC140 and is critical for assembly of the IC138 subcomplex, which contains IC138, IC97, LC7b, and FAP120, into Dynein-f (Hendrickson et al., 2004; Wirschell et al., 2007; Bower et al., 2009; VanderWaal et al., 2011). Mutation in IC138 affects the MT sliding velocity and flagellar waveform (VanderWaal et al., 2011). IC138 is hyperphosphorylated in *Chlamydomonas* paralyzed mutants with defective RSs (Habermacher and Sale, 1997; King and Dutcher, 1997; Yang and Sale, 2000; Hendrickson et al., 2004). Inhibitors of casein kinase 1 (CK1) or protein kinase A can block the phosphorylation and rescue MT sliding of the mutants (Howard et al., 1994; Yang and Sale, 2000; Smith, 2002; Wirschell et al., 2007). Therefore, it is proposed that, during the bending of flagella, RSs transmit mechano-chemical signals from the CP apparatus to ODAs and IDAs by modulating the phosphorylation state of IC138 and, thus, the regional Dynein-f activity (Smith and Yang, 2004; Wirschell et al., 2007).

Although composition and functions of axonenal dyneins have been extensively studied in unicellular protozoa such as *Chlamydomonas*, to what extent such knowledge can be applied

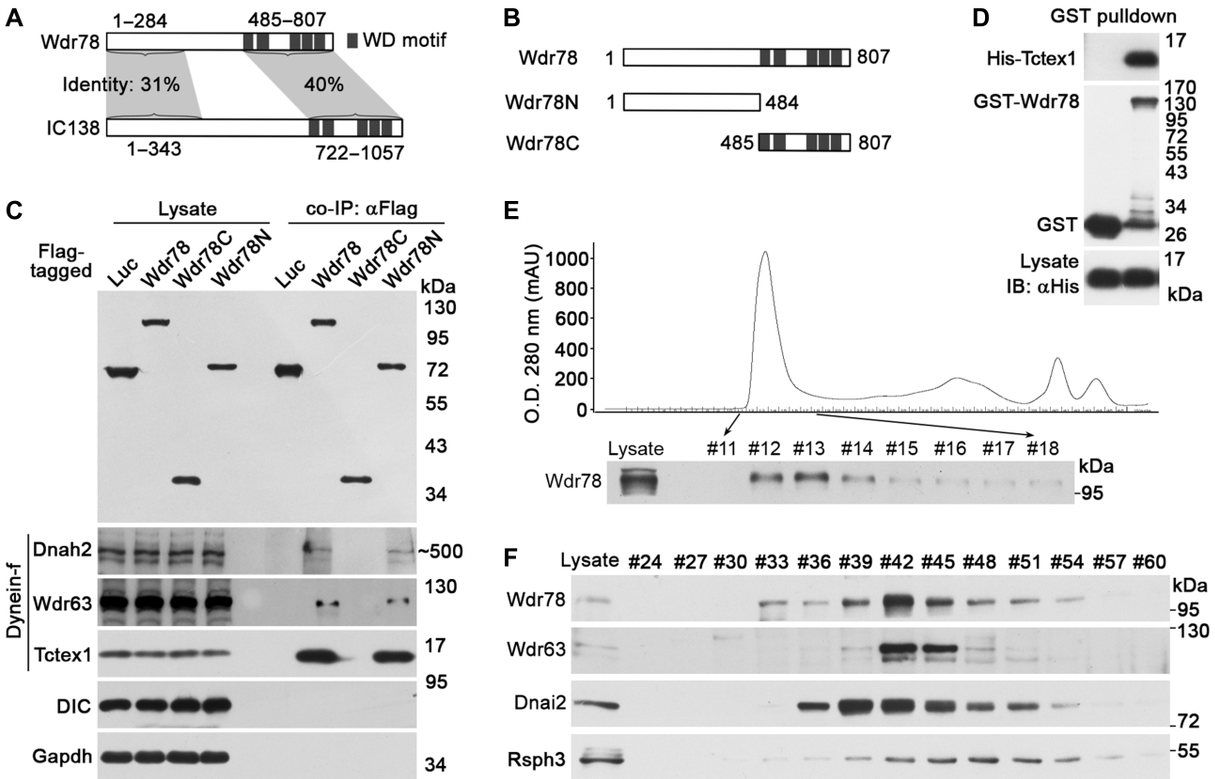

Figure 1 Wdr78 is homologous to IC138 and associates with multiple subunits of Dynein-f. (**A**) A comparison between Wdr78 and IC138. The numbers indicate amino acid positions. (**B**) Schematic diagrams of Wdr78 and mutants. The numbers indicate amino acid positions. (**C**) Associations of Flag-Wdr78 with Dynein-f in co-IP. Flag-tagged Wdr78 and its mutants expressed in HEK293T cells were used to co-immunoprecipitate their associated proteins from mouse testis lysates. DIC and Gapdh served as negative controls. (**D**) Tctex1 directly bound to Wdr78 *in vitro*. Bacterial lysates expressing the indicated proteins were mixed and subjected to GST pull-down assays. (**E** and **F**) Endogenous Wdr78 co-fractionated with Dynein-f in sequential column chromatography. Mouse testis lysates were applied to a size-exclusion Superose 6 10/300 GL column. (**E**) Eluted fractions were collected and subjected to immunoblotting to detect Wdr78. The fractions #12–#14 were combined and applied to an anion-exchange Mono Q 4.6/100 PE column. The bound proteins were eluted using a linear salt gradient. (**F**) The indicated fractions were analyzed by immunoblotting.

to vertebrate is poorly known. Not all dynein subunits are exactly conserved. For instance, *Chlamydomonas* ODA contains three HCs, each encoded by a single gene, whereas vertebrate ODA has two HCs but five different coding genes. Some IDA subunits also vary (Kobayashi and Takeda, 2012; Viswanadha et al., 2017). Furthermore, while Dynein-f is not essential for flagellar movement in *Chlamydomonas*, it is in *Trypanosoma brucei* (Springer et al., 2011), indicating that, even in protozoa, axonemal dyneins can contribute differently to ciliary motility. In this study, we investigated vertebrate Dynein-f mainly through characterization of the IC138 homologue Wdr78 and found that it differs significantly from its *Chlamydomonas* counterpart in functions and subunit dependency.

Results

Wdr78 is the vertebrate orthologue of IC138

To investigate the regulation and functions of Dynein-f in vertebrates, we first chose to characterize and explore the function of Wdr78, a vertebrate homologue of IC138 (Supplementary Figure S1) (Hom et al., 2011). Although murine Wdr78 is smaller by ~200 amino acids than *Chlamydomonas* IC138, both share 31% and 40% of identities at the N- and C-termini, respectively, and contain five WD40 motifs at the C-terminus (Figure 1A). To confirm that Wdr78 indeed associated with Dynein-f, we used Flag-Wdr78 expressed in HEK293T cells to immunoprecipitate its associated proteins from the lysates of adult mouse testis (Supplementary Figure S2A), which are abundant in motile cilia (sperm flagella). Mass spectrometric analysis identified multiple subunits of Dynein-f (Dnah2, Dnah10, Tctex1, and Wdr63), other IDAs (Dnah1, Dnah3, Dnah6, and Dnah12), and ODAs (Supplementary Figure S2B) (Hom et al., 2011) as the potential associated proteins. Among them, the peptide counts for the Dynein-f subunits Dnah2 (171 hits; 1α HC homologue), Wdr63 (113 hits; IC140 homologue), and Tctex1 (298 hits; light chain) (Chapelin et al., 1997; Harrison et al., 1998; Maiti et al., 2000; Hom et al., 2011) were the highest (Supplementary Figure S2B), suggesting preferential associations of Wdr78 with them.

We next constructed two Flag-tagged mutants, Wdr78N and Wdr78C (Figure 1B), and performed coimmunoprecipitation (co-IP) again, together with Flag-Wdr78, to validate the mass spectrometric results. Immunoblotting (IB) using available antibodies confirmed associations of Dnah2, Wdr63, and Tctex1 with Flag-Wdr78 (Figure 1C). Furthermore, these Dynein-f subunits associated with Wdr78N but not Wdr78C (Figure 1C). By contrast, neither Gapdh nor the IC of cytoplasmic dynein (DIC), to which Tctex1 also serves as a LC (Mok et al., 2001), was present in the immunoprecipitates (Figure 1C).

The high enrichment of Tctex1 in the immunoprecipitates of Wdr78 (Figure 1C and Supplementary Figure S2B) also prompted us to examine whether it could directly bind to Wdr78, though Tctex1 in *Chlamydomonas* is not considered as a direct binding protein of IC138 (VanderWaal et al., 2011). We expressed GST-Wdr78 and polyhistidine (His)-tagged Tctex1 in *Escherichia coli*. GST pull-down assays indicated a direct interaction between them (Figure 1D). When Flag-Wdr78 and HA-Tctex1 or HA-Dnal1, a homologue of the *Chlamydomonas* ODA LC1 (Tanner et al., 2008; Hom et al., 2011), were co-expressed in HEK293T cells and subjected to reciprocal co-IP using anti-Flag or anti-HA antibody, Flag-Wdr78 readily associated with HA-Tctex1 but not HA-Dnal1 (Supplementary Figure S2C), suggesting an interaction between Wdr78 and Tctex1 *in vivo*.

Next, we performed sequential column chromatography using the mouse testis lysates to examine the relationship among endogenous Wdr78 and other axonemal components. The lysates were initially loaded onto a size-exclusion column with a fractionation range of 5–5000 kDa and the Wdr78-containing complex was eluted in the first peak (fractions #12–#14) (Figure 1E). When fractions #12–#14 were pooled together and further resolved using an anion-exchange column, both Wdr78 and Wdr63 peaked in fractions #42 (Figure 1F). By contrast, Dnai2, an ODA IC (Hom et al., 2011), peaked in fraction #39, whereas Rsph3, peaked in fraction #48 (Figure 1F). Although we were unable to detect Dnah2 due to inadequate protein concentration, the co-fraction of Wdr78 with Wdr63 again supports its association with Dynein-f *in vivo*.

Mammalian Wdr78 is a motile cilia-specific protein

Wdr78 was highly enriched in mouse tissues containing motile cilia, including the trachea, lung, oviduct, and testis (Figure 2A). By contrast, the kidney and eye, tissues abundant in primary cilium, or cultured IMCD3 and NIH3T3 cells that had been induced by serum starvation to generate primary cilium contained low or undetectable levels of Wdr78 (Figure 2A).

In cultured mTECs induced to differentiate at an air–liquid interface (ALI), multiciliogenesis occurs from the second day post ALI (ALI d2) and reached plateau at around ALI d5 (Vladar and Stearns, 2007; Zhao et al., 2013; Xu et al., 2015). qRT-PCR analysis indicated that the mRNA levels of *Wdr78* correlated tightly with the multiciliogenesis (Figure 2B). Its expression pattern resembled those of other axonemal dynein subunits such as *Wdr63* and *Dnai2* but was distinct from those of *Plk4* and *Deup1*, which are important for basal body amplification (Figure 2B) (Habedanck et al., 2005; Zhao et al., 2013). Wdr78 also increased in accordance with the multiciliogenesis indicated by the elevated levels of Ift80 and acetylated tubulin (Figure 2C). Immunostaining showed that Wdr78 localized specifically in the axonomes of the multicilia of mTECs (Figure 2D) but was not detected in the primary cilia of NIH3T3 cells (Figure 2E).

Both mammalian Wdr78 and Dnah2 are essential for ciliary beat

Multiciliated mTECs are difficult for live imaging because they grow in transwells (Vladar and Stearns, 2007; Zhao et al., 2013). To understand the functions of Wdr78 in motile cilia, we isolated radial glial cells from P0 mice and induced them to differentiate into multiciliated mouse ependymal cells (mEPCs) by serum starvation (Spassky et al., 2005; Delgehyr et al., 2015) and depleted Wdr78 by RNAi (Figure 3A). Efficient depletion was achieved by using two independent siRNAs, 78-i1 and 78-i2 (Figure 3B and C).

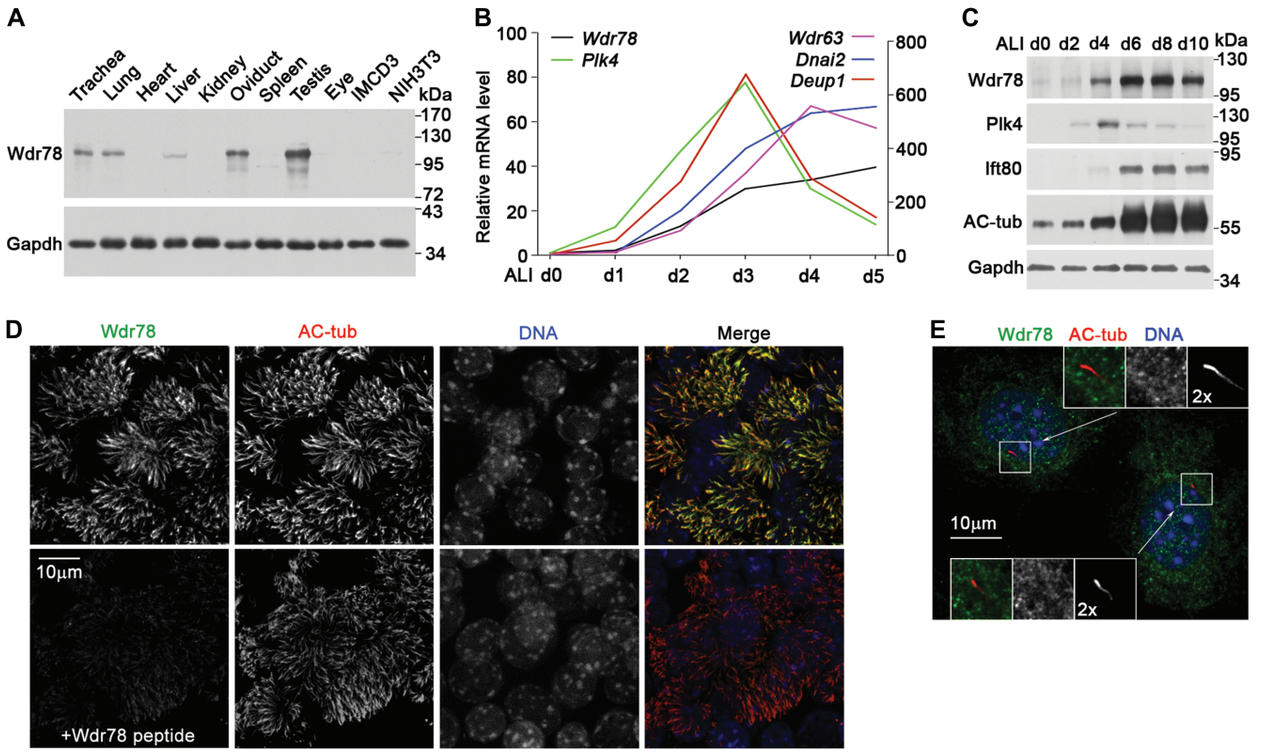

Figure 2 Wdr78 is located in motile cilia. (**A**) Wdr78 was highly expressed in motile cilia-containing tissues, including trachea, lung, oviduct, and testis. Cultured IMCD3 and NIH3T3 cells were serum-starved for 48 h to induce primary cilia. Gapdh served as loading control. (**B**) Expression profile of *Wdr78* during multiciliogenesis. qRT-PCR was performed using mRNAs extracted from mTECs cultured at an ALI for the indicated days (d). *Plk4* and *Deup1* served as markers for centriole amplification, whereas *Wdr63* and *Dnai2* served as markers for multiciliogenesis. The results were representative of two independent sets of experiments. (**C**) Protein levels of Wdr78 during the multiciliogenesis of mTECs. The increased levels of Ift80 and acetylated tubulin (AC-tub) indicate multiciliogenesis. Plk4 and Gapdh served as marker for centriole amplification and loading control, respectively. (**D**) Wdr78 localized in the axonemes of mTEC cilia. mTECs were fixed at ALI d7 and stained with anti-Wdr78 antibody preincubated with or without the Wdr78 peptide that was used for antibody generation. AC-tub marks ciliary axonemes. Nuclear DNA was stained with DAPI. (**E**) Wdr78 was not a primary ciliary protein. NIH3T3 cells were serum-starved for 48 h to induce primary ciliary formation. AC-tub marks ciliary axonemes. Nuclear DNA was stained with DAPI.

When examined using live imaging, multicilia in the majority of control mEPCs (91% on average) beat swiftly in a back-and-forth, or planar, manner (Figure 3D and E; Supplementary Video S1). Only 2% of the mEPCs contained immobile cilia (Figure 3E). By contrast, the depletion of Wdr78 severely impaired ciliary beating; 51% of the 78-i1-treated or 38% of the 78-i2-treated mEPCs on average displayed immobile multicilia (Figure 3D and E; Supplementary Video S1). In the remaining portions, 24%–26% contained slow beating cilia and 23%–38% contained fast beating cilia (Figure 3E), possibly due to inefficient RNAi.

To exclude the off-target effect of RNAi, we performed rescue experiments by expressing an RNAi-insensitive GFP-Wdr78 in 78-i2-treated mEPCs (Figure 3F). Compared to Centrin1-GFP, a centriolar protein serving as negative control (Figure 3F) (Zhao et al., 2013), GFP-Wdr78 significantly reduced the incidence of immobile cilia in the 78-i2-treated mEPCs from 53% to 12% on average (Figure 3G and H; Supplementary Video S2). Thus, depletion of Wdr78 causes PCD characterized by paralyzed cilia.

Next we depleted Dnah2 in mEPCs by RNAi using an efficient siRNA, Dnah2-i (Figure 3I). Live imaging indicated that 42% of the siRNA-treated mEPCs also displayed paralyzed multicilia (Figure 3J and K; Supplementary Video S3). In comparison, only 5% of the ctrl-i-treated mEPCs contained immobile cilia (Figure 3K). These results are consistent with those of Wdr78 depletion, though a rescue experiment is not practical due to the huge size of Dnah2 (>500 kDa).

Taken together, we conclude that Dynein-f is essential for ciliary beat of mEPCs.

Mammalian Wdr78 is required for Dynein-f assembly

To assess whether the depletion of Wdr78 affected ciliary localizations of other subunits of axonemal dynein, we established a protocol to purify motile cilia from cultured mEPCs (Figure 4A). The purified cilia were generally not fragmented and appeared to be structurally intact as suggested by the presence of the CP marker Hydin (Figure 4B) (Teves et al., 2016), though negative-staining electron microscopy revealed the

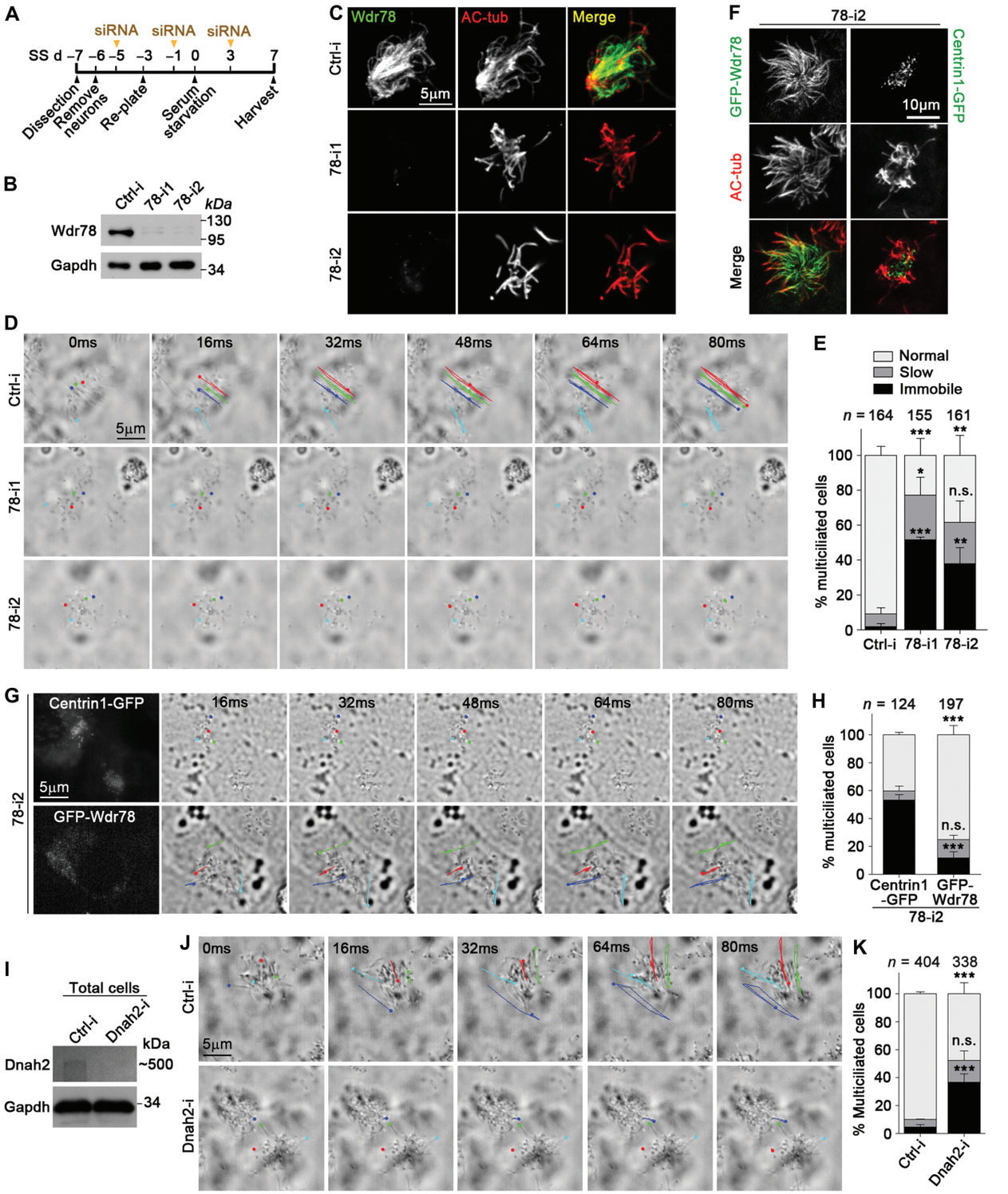

Figure 3 Vertebrate Dynein-f is critical for ciliary beat. (**A**) Experimental scheme for RNAi in mEPCs. Glial cells from dissected mouse telencephalon tissues were induced to differentiate into multiciliated mEPCs through serum starvation at day 0 (SS d0). The cells were transfected three times with siRNA. (**B** and **C**) Efficient knockdown of Wdr78 by RNAi. Gapdh and AC-tub served as loading control and ciliary marker, respectively. (**D** and **E**) Depletion of Wdr78 paralyzed ependymal cilia. Ciliary movements were monitored by bright-field microscopy. (**D**) Trajectories of four cilia during the first 80 ms of imaging are shown for each mEPC. Please also refer to Supplementary Video S1. (**F–H**)

existence of some vesicle-like contaminants (Figure 4C). Label-free quantitative (LFQ) proteomic analysis (Zhu et al., 2010) identified 841 and 875 proteins with LFQ intensities from the cilia samples purified from ctrl-i- and 78-i2-treated mEPCs, respectively. Among them, 767 proteins were overlapped. When the pool of 427 proteins identified through ≥5 unique peptides from the control cilia preparation was analyzed, 43% of them contained known ciliary proteins (Figure 4D). In comparison, only 8% were the Golgi, ER, and mitochondrial proteins, which most likely came from contaminants (Figure 4D), indicating a fine quality of the cilia preparation.

In the overlapped pool of 767 proteins, we found a 5.7-fold reduction of Wdr78 in the 78-i2-treated cilia (Figure 4E). Notably, four major Dynein-f subunits, Dnah10, Dnah2, Wdr63, and Casc1 (IC97 homologue, also named Las1) (King, 2016; Viswanadha et al., 2017), were also similarly reduced (Figure 4E). By contrast, HCs of other IDAs (e.g. Dnah1, Dnah3, Dnah6, and Dnah12) or ODAs (Dnah5, Dnah9, and Dnah11) (Hom et al., 2011; King, 2016; Viswanadha et al., 2017) and components of the RS (e.g. Rsph3 and Rsph9) (Pigino et al., 2011), the CP (Hydin and Spag16) (Teves et al., 2016), or intraflagellar transport complex (Ift52 and Ift140) (Prevo et al., 2017) were not altered as strikingly (Figure 4E). Immunoblotting of an independent set of samples confirmed the strong decrease of Wdr78 and Dnah2 in 78-i2-treated cilia (Figure 4F). These results suggest that the depletion of Wdr78 specifically impairs the ciliary assembly of Dynein-f.

Zebrafish Wdr78 morphants display ciliopathy-related phenotypes

To assess the physiological significance of Wdr78, we examined the effects of its knockdown on zebrafish embryonic development because ciliary defects are known to lead to various developmental disorders in zebrafish, including curved body, abnormal otolith (ear stone), hydrocephalus, and randomized left–right asymmetry (Riley et al., 1997; Essner et al., 2005; Kramer-Zucker et al., 2005; Wessely and Obara, 2008; Cao et al., 2012). We used two morpholino oligonucleotides (MOs), 78-MO^{ATG} and 78-MO^{SP}, to efficiently block the translation initiation of the *Wdr78* mRNA or splicing of its pre-mRNA, respectively (Supplementary Figure S3A–C). We found that, while embryos injected with a control MO (Ctrl-MO) developed normally, the *Wdr78* morphants produced a series of ciliopathy-related phenotypes (Figure 5). More than 80% of the *Wdr78* morphants exhibited conspicuously curved bodies at 72 h post fertilization (hpf), whereas only 4.5% had such a defect in the control group (Figure 5A and B). The incidences of hydrocephalus, pronephric cysts, or abnormal otoliths also increased at least 8-fold in the *Wdr78* morphants as compared with the control morphants (Figure 5C–H).

The left–right asymmetry was also perturbed in the *Wdr78* morphants. Normally the heart tube of zebrafish is oriented toward the left side (Yelon et al., 1999; Essner et al., 2005). When *in situ* hybridization of the mRNA of cardiac myosin light chain 2 (*cmlc2*) was performed to label the heart tube at 24–27 hpf (Yelon et al., 1999), we found that the heart tube was oriented correctly in 91.3% of control embryos but incorrectly toward the middle or the right in 61.2% of the 78-MO^{ATG}- or 41.9% of the 78-MO^{SP}-injected embryos (Figure 5I and J), suggesting a randomized left–right patterning of internal organs.

Zebrafish Wdr78 morphants show paralyzed pronephric cilia and abnormal beat of spinal cord cilia

We then examined ciliary motilities by using high-speed video microscopy. Pronephric cysts are often attributed to impaired motility of pronephric cilia, whereas the Kuppfer's vesicle (KV), a monociliated organ orthologous to the mammalian embryonic node, is critical for the left–right asymmetry (Essner et al., 2005; Kramer-Zucker et al., 2005). Both the KV and pronephric cilia contain '9 + 2' axonemes (Kramer-Zucker et al., 2005). Pronephric cilia beat in a coordinated pattern in control morphants at 60 hpf (Figure 5K and Supplementary Video S4) (Kramer-Zucker et al., 2005). *Wdr78* morphants still contained long pronephric cilia but they no longer showed coordinated ciliary beat (Supplementary Figure S3D and Video S5). Furthermore, paralyzed cilia (Figure 5K and Supplementary Video S5) were found in 33.3% of 78-MO^{ATG}- or 46.7% of 78-MO^{SP}-injected embryos but in none of the control embryos (n = 15 for each group). As the number of KV cilia was not significantly altered in the *Wdr78* morphants as compared with control embryos (Supplementary Figure S3E and F), we speculate that the abnormal heart tube orientations are also caused by aberrant ciliary motility (Essner et al., 2005; Kramer-Zucker et al., 2005).

The spinal cord cilia of zebrafish contain '9 + 0' axonemes and beat in a rotational fashion (Figure 5L and Supplementary Video S6) (Kramer-Zucker et al., 2005). In the *Wdr78* morphants, the spinal cord cilia beat irregularly and slowly (Figure 5L and Supplementary Video S7). Quantification indicated that the mean CBF was reduced from 20.0 Hz (Ctrl-MO) to 13.4 Hz (78-MO^{ATG}) and 13.1 Hz (78-MO^{SP}) (Figure 5M). These results suggest that vertebrate Dynein-f is important for the rotational beat pattern of the '9 + 0' type of motile cilia.

We also performed rescue experiments by co-injecting *in vitro* transcribed mRNA of Flag-tagged zebrafish Wdr78 (Flag-zWdr78). Nevertheless, although the plasmid used for the *in vitro* transcription was able to express Flag-zWdr78 in HEK293T cells, we were unable to detect the protein in zebrafish embryos at 24 hpf even when each of the embryos was injected with 500 pg of the *in vitro*

GFP-Wdr78, but not Centrin1-GFP, restored ciliary motility in 78-i2-treated mEPCs. In addition to the transfections with 78-i2 in **A**, the cells were also infected with lentivirus at SS d–2 to express an siRNA-resistant GFP-Wdr78 or Centrin1-GFP. (**F**) The ciliary localization of GFP-Wdr78 was obvious in fixed mEPCs. (**G**) Due to the difficulty to clearly capture the fluorescent images of rapidly beating cilia, live GFP-positive cells were identified by the fluorescence in their cell bodies. Please refer to Supplementary Video S2. (**I**–**K**) Depletion of Dnah2 also caused immobile cilia in mEPCs. Please refer to Supplementary Video S3. Quantification results in **E**, **H**, and **K** were from three independent experiments and presented as mean ± SD. Cell numbers analyzed are listed over each histogram. Student's *t*-test: n.s., not significant; *$P < 0.05$; **$P < 0.01$; ***$P < 0.001$.

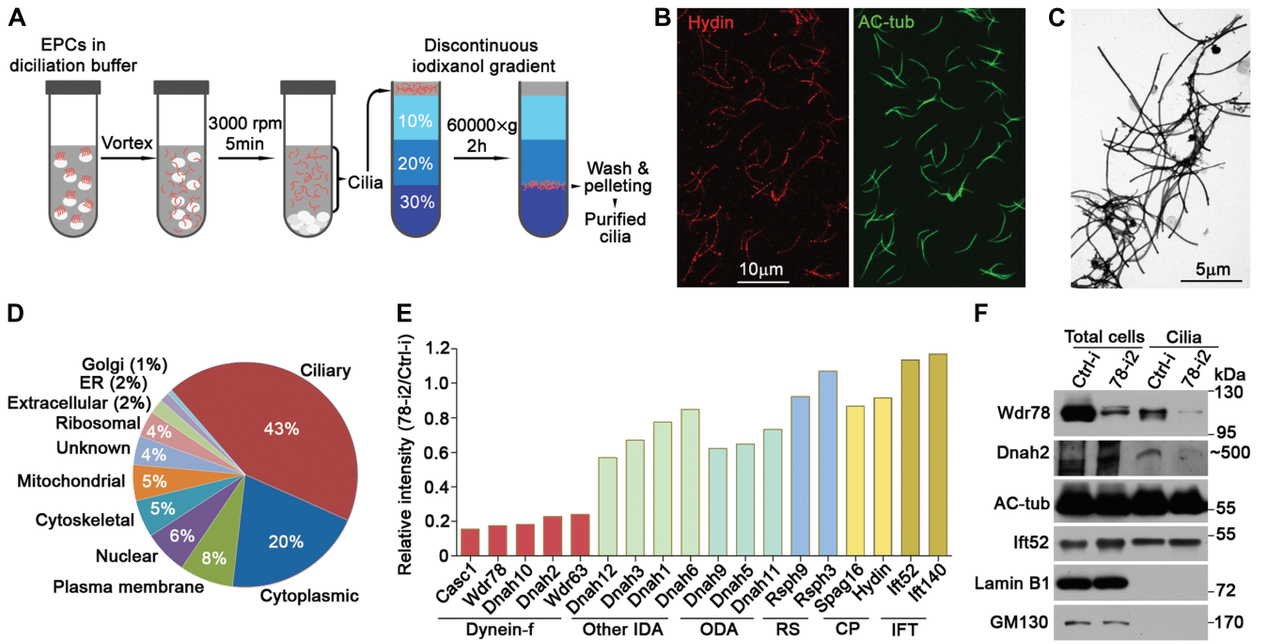

Figure 4 Wdr78 is required for ciliary assembly of Dynein-f. (**A**) Experimental scheme of ependymal cilia purification for LFQ mass spectrometric analysis. (**B** and **C**) Examination of purified cilia by immunofluorescence staining (**B**) and negative-staining electron microscopy (**C**). AC-tub- and Hydin-labeled axonemes and the CP, respectively. (**D**) Proteome analysis of a cilia preparation from Ctrl-i-treated mEPCs. Only hits with ≥5 unique peptides were included. (**E**) Relative LFQ intensities of the indicated proteins in 78-i2-treated cilia preparation, normalized to corresponding Ctrl-i-treated sample. (**F**) Dnah2 was markedly reduced in Wdr78-depleted ependymal cilia. AC-tub and Ift52 served as positive controls for the cilia preparations, whereas Lamin B1, a nuclear lamina protein, and GM130, a Golgi protein, served as negative controls. We failed to detect Wdr63 in the ciliary samples due to insufficient protein concentration.

transcribed mRNA (data not shown). Accordingly, when the mRNA was coinjected with the MOs, we were unable to observe a clear rescue effect on the body curvature. This is probably due to instability of the mRNA or its expressed Flag-zWdr78 in the developing embryos because the GFP-fusion protein expressed from the *in vitro* transcribed reporter mRNA was detected at 24 hpf after injection at 100 pg/embryo (Supplementary Figure S3B).

Discussion

In this study, we provide several lines of evidence to confirm that Wdr78 is an IC of vertebrate Dynein-f. First, Wdr78 was homologous to and shared similar structural features with IC138, an IC of *Chlamydomonas* Dynein-f (Figure 1A and Supplementary Figure S1) (Hendrickson et al., 2004; Wirschell et al., 2007; Bower et al., 2009). Second, it preferentially associated with other Dynein-f subunits, including HC (Dnah2), IC (Wdr63), and LC (Tctex1) (Figure 1B–F and Supplementary Figure S2). Third, it was a motile cilium-specific protein (Figure 2). Finally and most importantly, depletion of Wdr78 by RNAi in mEPCs selectively disrupted ciliary localizations of other Dynein-f subunits, such as the HCs (Dnah10 and Dnah2) and the ICs (Wdr63 and Casc1) (Figure 4). Our results also provide the first experimental evidence that validates Dnah10 and Dnah2 as HCs and Wdr78, Wdr63, and Casc1 as ICs of vertebrate Dynein-f because their assignments before are solely based on sequence homologies with *Chlamydomonas* 1α HC, 1β HC, IC138, IC140, and IC97, respectively (Hom et al., 2011; King, 2016; Viswanadha et al., 2017).

We found that Dynein-f plays a more important role in vertebrate ciliary motility than in *Chlamydomonas*. Depletion of either Wdr78 or Dnah2 by RNAi in mEPCs caused PCD with markedly increased incidences of immotile cilia (Figure 3; Supplementary Videos S1 and S3). Ectopically expressed Wdr78 rescued the motility defect of the 78-i2-treated cilia (Figure 3F–H and Supplementary Video S2), thus excluded off-target effect. Paralyzed cilia were also common in the pronephros of zebrafish Wdr78 morphants as compared with the control (Figure 5K; Supplementary Videos S4 and S5). As the existence of mobile cilia could be attributed to incomplete depletion (Figure 4E and F), our results strongly suggest that vertebrate Dynein-f is essential for the motility of the '9 + 2' type of cilia. This is in sharp contrast to its *Chlamydomonas* counterpart (Myster et al., 1997, 1999; VanderWaal et al., 2011). Thus, metazoan Dynein-f appears to use the *Trypanosoma* counterpart (Springer et al., 2011), but not the *Chlamydomonas* one, as its prototype during evolution. In addition, the irregular beating and reduced CBFs of the spinal cord cilia in the zebrafish *Wdr78* morphants (Figure 5L and M; Supplementary Videos S6 and S7) suggest a critical role of vertebrate Dynein-f in the '9 + 0' type of motile cilia. The widespread ciliopathy-related phenotypes in the morphants suggest that Wdr78 mutations in human may cause ciliopathies as well.

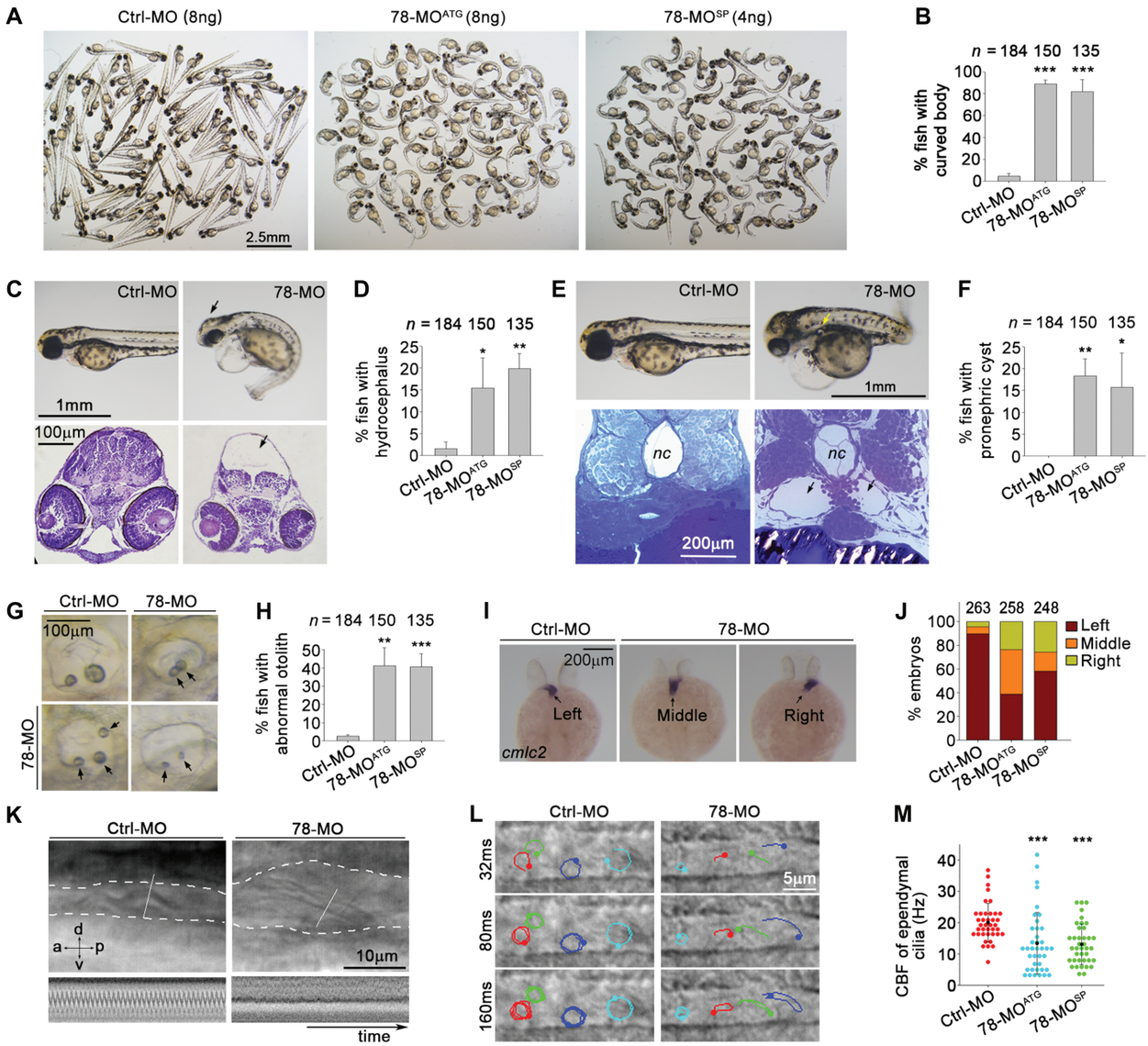

Figure 5 Phenotypes of zebrafish *Wdr78* morphants. (**A** and **B**) Body curvatures at 72 hpf. Ctrl-MO, the standard control morpholino; 78-MO^{ATG} and 78-MO^{sp}, two antisense MOs targeting the translation initiation site and a splicing site of *Wdr78* mRNA, respectively. The same populations were also used for assays in **C**–**H**. (**C** and **D**) Hydrocephalus (arrows). (**E** and **F**) Pronephric cysts (arrows). *nc*, notochore. (**G** and **H**) Abnormal number, size, or positioning of otoliths (arrows). (**I** and **J**) Randomized heart tube orientations. Whole-mount *in situ* hybridization of *Cmlc2* mRNA was performed to label the heart tube (arrows) at 24–27 hpf. (**K**) Impaired motility of pronephric cilia. Motility of pronephric cilia, recorded at 250 frames per sec (fps) as differential-interference-contrast images at 60 hpf, is presented in Supplementary Videos S4 and S5. The first frames of the videos, with the pronephric duct outlined with dashed lines and kymographs of the cilia at the position of the white lines are shown here. a, anterior; d, dorsal; p, posterior; v, ventral. (**L** and **M**) Impaired motility of spinal cord cilia. Motilities of spinal cord cilia were recorded at 250 fps at 60 hpf. Trajectories of four cilia during the first 160 ms of imaging are shown for each embryo. Please refer to Supplementary Videos S6 and S7. The CBFs of three traceable cilia were quantified for each of 13 morphants in each group. Note that immobile cilia, if any, were difficult to identify in the images due to high backgrounds. Quantification results were from three independent experiments and presented as mean ± SD. Embryo numbers analyzed are listed over each histogram. Student's *t*-test: $*P < 0.05$; $**P < 0.01$; $***P < 0.001$.

Wdr78 also acquires novel functions. IC138 does not contribute to the flagellar assembly of the HCs and IC140 in *Chlamydomonas* (Hendrickson et al., 2004; Wirschell et al., 2007; Bower et al., 2009; VanderWaal et al., 2011). Wdr78, however, is required for the ciliary assembly of the entire Dynein-f (Figure 4). It also becomes directly binding to Tctex1

(Figure 1D and Supplementary Figure S2C), which is not considered as an interacting LC of IC138 (Bower et al., 2009; VanderWaal et al., 2011; Viswanadha et al., 2017). Furthermore, although IC138/Wdr78, IC140/Wdr63, and IC97/Casc1 are conserved in evolution, FAP120, a subunit in the IC138 subcomplex, does not contain a homologue in vertebrate (King, 2016; Viswanadha et al., 2017). Therefore, vertebrate Dynein-f is assembled differently from its *Chlamydomonas* counterpart to probably comply with ciliary roles in higher organisms. Since almost all of our current knowledge on Dynein-f and many other motile cilia-related machineries come from protozoan model systems, our findings also point out the importance for studies in vertebrate systems in order to achieve full understandings on molecular mechanisms underlying ciliary motilities and the etiology of ciliopathies.

What changes at the molecular level resulting in the functional discrepancies between Wdr78 and IC138 is currently unclear. *Chlamydomonas* IC138 is longer than vertebrate Wdr78 by more than 200 amino acid residues (Supplementary Figure S1). Its four large regions of over 25 residues each are deleted in the vertebrate Wdr78, in addition to several smaller ones (Supplementary Figure S1). Furthermore, the overall sequence identities between them are only approximately 30%. Although these sequence differences are in agreement with the functional divergence of the proteins, their detailed physiological meanings will require future studies to elucidate.

Materials and methods

Plasmids and siRNA

The cDNAs of Wdr78 (Genbank accession NM_146254.4), Tctex1 (NM_009342.2), and Dnal1 (NM_028821.3) were amplified by PCR from reverse-transcribed mouse testis total cDNAs. The PCR fragments were cloned into pcDNA3.1-NFlag, pcDNA3-HA, pGEX-4T-1, or pET28a for the expression of Flag-, GST-, or His-tagged proteins. To generate lentiviral constructs for the expression of 78-i2-resistant Wdr78, whose coding sequences GTCTGAAGAAGCTGAGAAA were mutated into ATCAGAGGAGG CAGAAAAA by PCR without changing the coding amino acids, and Centrin1 (NM_007593.5) for rescue experiments, the PCR fragments were inserted into pLKO.1 modified by replacing the puromycin-resistance gene with a cDNA encoding GFP (Zhao et al., 2013). All the constructs were verified by sequencing.

The siRNA targeting sequences were 5′-TTCTCCGAACGTGTCACGT-3′ for Ctrl-i, 5′-GGACAGTAGTGAATCACCT-3′ for 78-i1, 5′-GTCTGAAG AAGCTGAGAAA-3′ for 78-i2, and 5′-CCCAAACTCTTCACAGAAT-3′ for Dnah2-i.

Antibodies

Rabbit antibody against mouse Wdr78 or Dnah2 were generated against peptide YLETYRGHKGPVYK or YGKLRDTIEQEIR, respectively, and affinity-purified (Abgent) for immunoblotting and immunofluorescence staining. Rabbit antibody against mouse Wdr78 was raised using bacterially expressed His-Wdr78 (1–420 amino acids) and then affinity-purified using GST-Wdr78 (1–420 amino acids) for IP. Rabbit anti-Plk4 antibody was prepared as described (Zhao et al., 2013). Commercial mouse monoclonal antibodies used were acetylated tubulin (Sigma, T6793), GST (Wolwo, Mab-GS01), His (Sigma, H1029), Tctex1 (Millipore, MAB1076), DIC74.1 (Millipore, MAB1618), Dnai2 (Abnova, H00064446-M01), and GM130 (BD, 610823). Commercial rabbit antibodies used were Flag (Sigma, F7425), Ift80 (GeneTex, GTX109393), Ift52 (Proteintech, 17534-1-AP), Rsph3 (Proteintech, 17603-1-AP), GFP (Life Technologies, A6455), Wdr63 (GeneTex, GTX45697), Lamin B1 (Proteintech,12987-1-AP), and Gapdh (Proteintech, 10494-1-AP). Secondary antibodies conjugated with peroxidase or Alexa Fluor-488, -546, or -647 were purchased from Life Technologies. Conformation-specific mouse anti-rabbit IgG mAb conjugated with peroxidase was purchased from Cell Signaling Technology (L27A9). Anti-Flag M2 resin and glutathione agarose beads were from Sigma. Recombinant protein G (rProtein G) agarose beads were from Life Technologies.

Cell culture, viral production, and transfection

HEK293T cells were maintained in DMEM (Hyclone) supplemented with 10% fetal bovine serum (Biochrom), 0.3 mg/ml glutamine (Sigma), 100 U/ml penicillin (Invitrogen), and 100 mg/ml streptomycin (Invitrogen) at 37°C in an atmosphere containing 5% CO_2. To express exogenous proteins for biochemical assays, HEK 293 T cells were transfected using the calcium phosphate method for 48 h. Lentiviral production was performed as described (Zhao et al., 2013).

Multiciliated mTECs were isolated and cultured as described previously (You et al., 2002; Zhao et al., 2013). Multiciliated mEPCs were obtained as described (Mirzadeh et al., 2008; Guirao et al., 2010), with minor modifications. Briefly, the telencephala of P0 C57BL/6J mice were dissected and digested for 30 min with freshly prepared papain solution (10000 U/ml; Worthington Biochemical Corp.) at 37°C. After gentle pipetting with a P1000 tip and centrifugation at 1400 rpm for 5 min at room temperature, the pelleted cells were resuspended in the culture medium (DMEM plus 10% FBS) and seeded into 25-cm^2 laminin-coated flasks (1 brain/flask) at SS d–7. After culturing for 1 day, neurons were shaken off and removed. The remaining radial glia-enriched cells were further cultured to ~80% confluency (usually 3 days) and then transferred into the wells of laminin-coated 29-mm glass-bottom dishes (Cellvis, D29-14-1.5-N) at a density of 2×10^5 cells per well (SS d–3). The cells grown in the culture medium for another 3 days were then maintained in serum-free medium (serum starvation) to induce multicilia formation (SS d0). Multiciliated mEPCs were used for imaging or other assays at SS d7.

For Wdr78 RNAi, siRNAs were transfected into radial glia or mEPCs using Lipofectamine RNAiMAX (Life Technologies) at SS d–5, d–1, and d3, respectively. For Dnah2 RNAi, siRNAs were transfected at SS d–1 and d3, respectively, and 4 μl of the oligonucleotides (20 μM) and 6 μl of Lipofectamine were used for a well of cells. For rescue experiments, in addition to the transfections with siRNA, the cells were infected with lentivirus at SS d–2 to express GFP-tagged RNAi-insensitive Wdr78 or Centrin1.

Quantitative RT-PCR

qRT-PCR was performed as described previously with minor modifications (Xu et al., 2015). Briefly, 2 μg of total RNA was used for each reverse transcription reaction using the Superscript III First Strand Synthesis System with oligo-dT primers (Life Technologies). qPCR was performed by using an Applied Biosystems 7500 HT Sequence Detection System with the Power SYBR Green PCR Master Mix Kit (Applied Biosystems). Gapdh served as internal control.

Purification of ependymal cilia

Three 75-cm^2 flasks of the 78-i2-treated or Ctrl-i-treated mEPCs were harvested at SS d7 by centrifugation at 2000 rpm for 5 min at 4°C. The cells were resuspended in 2.4 ml of deciliation buffer (20 mM PIPES, pH 5.5, 250 mM sucrose, 20 mM $CaCl_2$, 0.05% Triton X-100) and agitated vigorously for 10 min on a vortex mixer (G560OE, Scientific Industries). After centrifugation at 3000 rpm for 5 min at 4°C, the supernatant, which contained cilia, was collected. This step was repeated once. The cilia-containing supernatant was then loaded on top of a discontinuous gradient of iodixanol (OptiPrep™, 10%, 20%, and 30%) in PBS and centrifuged at 60000× *g* for 2 h. The cilia enriched at the interface between the 20% and 30% iodixanol layers were carefully collected. The collection was diluted by 4-fold with PBS and centrifuged at 20000× *g* for 30 min. The pelleted cilia were washed twice with 1 ml of PBS, followed by centrifugation at 20000× *g* for 15 min. The cilia were lysed in 110 μl of lysis buffer (20 mM Tris-HCl, pH 7.5, 100 mM KCl, 0.1% NP-40, 1 mM EDTA, 10 mM $Na_4O_7P_2$, and protease inhibitors) and boiled for 10 min. The samples were subjected to mass spectrometric or immunoblotting analyses.

Light microscopy

Fluorescence microscopy was carried out as described previously (Cao et al., 2012; Zhao et al., 2013). Multiciliated mTECs or mEPCs were pre-extracted with PBS containing 0.5% Triton X-100 for 1 min followed by fixation with 4% paraformaldehyde in PBS for 15 min at room temperature. Purified cilia were spun onto a coverslip pretreated with 10 μg/ml poly-D-lysine with a swing-out rotor at 5300 rpm for 30 min at 4°C, and then fixed with 4% paraformaldehyde in PBS for 10 min. For competition experiments, 1 μg of anti-Wdr78 antibody was preincubated with 10 μg of immunogen for 2 h at room temperature before used for immunostaining. Whole-mount immunostaining of zebrafish embryos was performed as described (Wloga et al., 2009; Cao et al., 2012). Fluorescent images were captured using a SZX16 stereomicroscope (Olympus), BX51 microscope (Olympus), or TCS SP5 laser-scanning confocal microscope (Leica).

High-speed video microscopy for cilia motility was performed with a 63× objective on an IX71 microscope (Olympus) equipped with a Neo sCMOS camera (Andor). mEPCs at SS d7 were imaged at 125 fps for 2 sec. Zebrafish embryos were imaged at 250 fps for 2 sec as described (Kramer-Zucker et al., 2005). Ciliary trajectories were illustrated with the manual tracking plugin in the Image J software. Four traceable cilia in each cell were tracked over a period of 80 ms (mEPCs) or 160 ms (zebrafish). The CBF of each cilium was calculated from the overall time of 10 beating cycles.

Electron microscopy

The purified cilia (5 μl) were loaded onto a carbon grid and let it stand for 1 min at room temperature. After removing the liquid, the sample was stained with 2% uranyl acetate for 1 min. Electron microscope (EM) images were acquired with a Tecnai Spirit 120 kV transmission EM (FEI).

Immunoprecipitation and GST pull-down

Immunoprecipitations were carried out as described (Shen et al., 2008). Testis from 8-week-old C57BL/6J mice were sliced and lysed with a glass homogenizer in cold lysis buffer [20 mM Tris-HCl, pH 7.5, 0.1% NP-40, 100 mM KCl, 50 mM NaF, 10 mM $Na_4O_7P_2$, 1 mM Na_3VO_4, 1 mM EDTA, 10% Glycerol, 1 mM DTT, 1 mM PMSF, plus protease inhibitors cocktail (Calbiochem, 539134)]. The tissue lysate was collected after spinning for 10 min at 13,000 rpm at 4°C to remove debris. HEK293T cells transiently expressing Flag-tagged luciferase, Wdr78 or its mutants were lysed similarly and mixed respectively with an aliquot of the testis lysate. The mixtures were incubated for 2 h at 4°C under rotary agitation to allow complex formation between Flag-Wdr78 and axonemal proteins. Anti-Flag M2 resin (Sigma) was then added for additional 2 h of rotary incubation. After six times of wash, elution was performed using Flag peptide.

For GST pull-down assays, bacterial lysates containing GST- or His-tagged fusion proteins were premixed for 1 h at 4°C and then incubated with glutathione agarose beads (Sigma-Aldrich) for another 2 h under rotary agitation. After six times of wash, the beads were boiled in SDS-sample buffer and subjected to immunoblotting.

Column chromatography

Eight-week-old mouse testis were homogenized in HMDEK buffer (30 mM HEPES, pH 7.4, 5 mM MgSO4, 1 mM DTT, 0.5 mM EGTA, 1% glycerol, 25 mM KCl) containing 0.1% NP-40, 10 μg/ml nocodazole, and proteinase inhibitors (PMSF and cocktail) (Sloboda, 2009). The lysates were cleared by centrifugation at 13000 rpm at 4°C for 30 min and filtered through a 0.22-μm filter. The solution was loaded on a prepacked Superose 6 10/300 GL column (GE Healthcare) on a GE AKTA Purifier FPLC system at 4°C. Elution was performed with HMDEK buffer at a flow rate of 0.5 ml/min. Fractions #12–#14 that were abundant in Wdr78 were pooled and applied to an anion-exchange column (Mono Q 4.6/100 PE, GE Healthcare). The bound proteins were eluted with a linear salt gradient of 0.2–1.0 M KCl in HMDEK buffer at a flow rate of 0.5 ml/min. The 0.5-ml fractions were collected for immunoblotting.

Microinjection of zebrafish embryos

MOs capable of blocking either the mRNA translation (78-MO^{ATG}: 5′-TCTGTGTGACTGTTGTGTTAGACAT-3′) or pre-mRNA

splicing (78-MO^{SP}: 5′-AAGACTGCTCACAGCCCCACCTGCT-3′) of zWdr78 were designed and purchased from Gene Tools (Philomath). The Morpholino Standard Control (Gene Tools) was used as control (Ctrl-MO). The MOs were dissolved in nuclease-free water and injected at 2 nl (4 or 8 ng) per embryo into the yolk at the one- or two-cell stage using a Narishige IM300 microinjector. Phenol red (0.02%) and GFP mRNA (50 pg) transcribed *in vitro* were coinjected as tracers (Cao et al., 2012).

To validate the knockdown efficiency of 78-MO^{ATG}, a 120-bp fragment of zWdr78 containing the MO-targeting sequence was PCR amplified from full-length cDNA (Open Biosystems) and inserted in-frame into pEGFP-N1 (Clontech) to create a GFP reporter. A cDNA fragment containing the entire reporter-coding sequence was subsequently cloned into pCS2+ for *in vitro* mRNA transcription (Cao et al., 2012). GFP reporter mRNA (100 pg) were coinjected with 8 ng of 78-MO^{ATG} per embryo and imaged at 24 hpf. The efficiency of 78-MO^{SP} was determined by RT-PCR (primers: 5′-GGGATATGGACAGGTTGAGT-3′; 5′-ATTCTTCCATCAG ACGACAC-3′). zGapdh served as the internal control (primers: 5′-TGTGATGGGAGTCAACCAGGACAA-3′; 5′-TTAGCCAGAGGAGCC AAGCAGTTA-3′).

In situ hybridization and histology

Whole-mount *in situ* hybridization of zebrafish embryos was performed as described previously (Wloga et al., 2009; Cao et al., 2012). For tissue histology, zebrafish embryos at 72 hpf were fixed overnight with 4% paraformaldehyde in PBS at 4°C, dehydrated serially with ethanol, cleared in dimethyl benzene, and embedded in paraffin wax. The embryos were sectioned at 5-μm thickness. Slides were stained in hematoxylin and eosin.

Data analyses

GraphPad Prism software was used for statistical analyses. Statistical results from three or more independent experiments were subjected to two-tailed Student's *t*-test. Differences were considered significant when $P < 0.05$.

Supplementary material

Supplementary material is available at *Journal of Molecular Cell Biology* online.

Acknowledgements

The authors thank Zhili Wu and Tianqing Zhang for technical assistances on zebrafish microinjection and EM and thank the NCPSS mass spectrometry system, institutional core facilities for cell biology and molecular biology for instrumental and technical supports.

Funding

This work was equally supported by the National Natural Science Foundation of China (NSFC; 31330045), the National Key R&D Program of China (2017YFA0503500), and Chinese Academy of Sciences (XDB19020000). It was also supported by NSFC (31471323) to X.Y.

Conflict of interest: none declared.

References

Bower, R., VanderWaal, K., O'Toole, E., et al. (2009). IC138 defines a subdomain at the base of the I1 dynein that regulates microtubule sliding and flagellar motility. Mol. Biol. Cell *20*, 3055–3063.

Brokaw, C.J., and Kamiya, R. (1987). Bending patterns of Chlamydomonas flagella: IV. Mutants with defects in inner and outer dynein arms indicate differences in dynein arm function. Cell Motil. Cytoskeleton *8*, 68–75.

Brooks, E.R., and Wallingford, J.B. (2014). Multiciliated cells. Curr. Biol. *24*, R973–R982.

Cao, J., Shen, Y., Zhu, L., et al. (2012). miR-129-3p controls cilia assembly by regulating CP110 and actin dynamics. Nat. Cell Biol. *14*, 697–706.

Chapelin, C., Duriez, B., Magnino, F., et al. (1997). Isolation of several human axonemal dynein heavy chain genes: genomic structure of the catalytic site, phylogenetic analysis and chromosomal assignment. FEBS Lett. *412*, 325–330.

Delgehyr, N., Meunier, A., Faucourt, M., et al. (2015). Ependymal cell differentiation, from monociliated to multiciliated cells. Methods Cell Biol. *127*, 19–35.

Essner, J.J., Amack, J.D., Nyholm, M.K., et al. (2005). Kupffer's vesicle is a ciliated organ of asymmetry in the zebrafish embryo that initiates left-right development of the brain, heart and gut. Development *132*, 1247–1260.

Fliegauf, M., Benzing, T., and Omran, H. (2007). When cilia go bad: cilia defects and ciliopathies. Nat. Rev. Mol. Cell Biol. *8*, 880–893.

Guirao, B., Meunier, A., Mortaud, S., et al. (2010). Coupling between hydrodynamic forces and planar cell polarity orients mammalian motile cilia. Nat. Cell Biol. *12*, 341–350.

Habedanck, R., Stierhof, Y.D., Wilkinson, C.J., et al. (2005). The Polo kinase Plk4 functions in centriole duplication. Nat. Cell Biol. *7*, 1140–1146.

Habermacher, G., and Sale, W.S. (1997). Regulation of flagellar dynein by phosphorylation of a 138-kD inner arm dynein intermediate chain. J. Cell Biol. *136*, 167–176.

Harrison, A., Olds-Clarke, P., and King, S.M. (1998). Identification of the t complex-encoded cytoplasmic dynein light chain tctex1 in inner arm I1 supports the involvement of flagellar dyneins in meiotic drive. J. Cell Biol. *140*, 1137–1147.

Hendrickson, T.W., Perrone, C.A., Griffin, P., et al. (2004). IC138 is a WD-repeat dynein intermediate chain required for light chain assembly and regulation of flagellar bending. Mol. Biol. Cell *15*, 5431–5442.

Hom, E.F., Witman, G.B., Harris, E.H., et al. (2011). A unified taxonomy for ciliary dyneins. Cytoskeleton *68*, 555–565.

Howard, D.R., Habermacher, G., Glass, D.B., et al. (1994). Regulation of Chlamydomonas flagellar dynein by an axonemal protein kinase. J. Cell Biol. *127*, 1683–1692.

Ishikawa, T. (2012). Structural biology of cytoplasmic and axonemal dyneins. J. Struct. Biol. *179*, 229–234.

Kamiya, R. (2002). Functional diversity of axonemal dyneins as studied in Chlamydomonas mutants. Int. Rev. Cytol. *219*, 115–155.

King, S.M. (2012). Integrated control of axonemal dynein AAA^{+} motors. J. Struct. Biol. *179*, 222–228.

King, S.M. (2016). Axonemal dynein arms. Cold Spring Harb. Perspect. Biol. *8*, pii: a028100.

King, S.J., and Dutcher, S.K. (1997). Phosphoregulation of an inner dynein arm complex in Chlamydomonas reinhardtii is altered in phototactic mutant strains. J. Cell Biol. *136*, 177–191.

Kobayashi, D., and Takeda, H. (2012). Ciliary motility: the components and cytoplasmic preassembly mechanisms of the axonemal dyneins. Differentiation *83*, S23–S29.

Kramer-Zucker, A.G., Olale, F., Haycraft, C.J., et al. (2005). Cilia-driven fluid flow in the zebrafish pronephros, brain and Kupffer's vesicle is required for normal organogenesis. Development *132*, 1907–1921.

Maiti, A.K., Mattei, M.G., Jorissen, M., et al. (2000). Identification, tissue specific expression, and chromosomal localisation of several human dynein heavy chain genes. Eur. J. Hum. Genet. *8*, 923–932.

Mirzadeh, Z., Merkle, F.T., Soriano-Navarro, M., et al. (2008). Neural stem cells confer unique pinwheel architecture to the ventricular surface in neurogenic regions of the adult brain. Cell Stem Cell *3*, 265–278.

Mizuno, N., Taschner, M., Engel, B.D., et al. (2012). Structural studies of ciliary components. J. Mol. Biol. *422*, 163–180.

Mok, Y.K., Lo, K.W., and Zhang, M. (2001). Structure of Tctex-1 and its interaction with cytoplasmic dynein intermediate chain. J. Biol. Chem. *276*, 14067–14074.

Myster, S.H., Knott, J.A., O'Toole, E., et al. (1997). The Chlamydomonas Dhc1 gene encodes a dynein heavy chain subunit required for assembly of the I1 inner arm complex. Mol. Biol. Cell *8*, 607–620.

Myster, S.H., Knott, J.A., Wysocki, K.M., et al. (1999). Domains in the 1α dynein heavy chain required for inner arm assembly and flagellar motility in Chlamydomonas. J. Cell Biol. *146*, 801–818.

Nicastro, D., Schwartz, C., Pierson, J., et al. (2006). The molecular architecture of axonemes revealed by cryoelectron tomography. Science *313*, 944–948.

Pigino, G., Bui, K.H., Maheshwari, A., et al. (2011). Cryoelectron tomography of radial spokes in cilia and flagella. J. Cell Biol. *195*, 673–687.

Praveen, K., Davis, E.E., and Katsanis, N. (2015). Unique among ciliopathies: primary ciliary dyskinesia, a motile cilia disorder. F1000Prime Rep. *7*, 36.

Prevo, B., Scholey, J.M., and Peterman, E.J.G. (2017). Intraflagellar transport: mechanisms of motor action, cooperation, and cargo delivery. FEBS J. *284*, 2905–2931.

Riley, B.B., Zhu, C.W., Janetopoulos, C., et al. (1997). A critical period of ear development controlled by distinct populations of ciliated cells in the zebrafish. Dev. Biol. *191*, 191–201.

Satir, P., and Christensen, S.T. (2007). Overview of structure and function of mammalian cilia. Annu. Rev. Physiol. *69*, 377–400.

Shen, Y., Li, N., Wu, S., et al. (2008). Nudel binds Cdc42GAP to modulate Cdc42 activity at the leading edge of migrating cells. Dev. Cell *14*, 342–353.

Sloboda, R.D. (2009). Purification and localization of intraflagellar transport particles and polypeptides. Methods Mol. Biol. *586*, 207–225.

Smith, E.F. (2002). Regulation of flagellar dynein by the axonemal central apparatus. Cell Motil. Cytoskeleton *52*, 33–42.

Smith, E.F., and Yang, P. (2004). The radial spokes and central apparatus: mechano-chemical transducers that regulate flagellar motility. Cell Motil. Cytoskeleton *57*, 8–17.

Spassky, N., Merkle, F.T., Flames, N., et al. (2005). Adult ependymal cells are postmitotic and are derived from radial glial cells during embryogenesis. J. Neurosci. *25*, 10–18.

Springer, A.L., Bruhn, D.F., Kinzel, K.W., et al. (2011). Silencing of a putative inner arm dynein heavy chain results in flagellar immotility in Trypanosoma brucei. Mol. Biochem. Parasitol. *175*, 68–75.

Tanner, C.A., Rompolas, P., Patel-King, R.S., et al. (2008). Three members of the LC8/DYNLL family are required for outer arm dynein motor function. Mol. Biol. Cell *19*, 3724–3734.

Teves, M.E., Nagarkatti-Gude, D.R., Zhang, Z., et al. (2016). Mammalian axoneme central pair complex proteins: broader roles revealed by gene knockout phenotypes. Cytoskeleton *73*, 3–22.

VanderWaal, K.E., Yamamoto, R., Wakabayashi, K., et al. (2011). bop5 mutations reveal new roles for the IC138 phosphoprotein in the regulation of flagellar motility and asymmetric waveforms. Mol. Biol. Cell *22*, 2862–2874.

Viswanadha, R., Sale, W.S., and Porter, M.E. (2017). Ciliary motility: regulation of axonemal dynein motors. Cold Spring Harb. Perspect. Biol. *9*, pii: a018325.

Vladar, E.K., and Stearns, T. (2007). Molecular characterization of centriole assembly in ciliated epithelial cells. J. Cell Biol. *178*, 31–42.

Wessely, O., and Obara, T. (2008). Fish and frogs: models for vertebrate cilia signaling. Front. Biosci. *13*, 1866–1880.

Wirschell, M., Hendrickson, T., and Sale, W.S. (2007). Keeping an eye on I1: I1 dynein as a model for flagellar dynein assembly and regulation. Cell Motil. Cytoskeleton *64*, 569–579.

Wloga, D., Webster, D.M., Rogowski, K., et al. (2009). TTLL3 Is a tubulin glycine ligase that regulates the assembly of cilia. Dev. Cell *16*, 867–876.

Xu, Y., Cao, J., Huang, S., et al. (2015). Characterization of tetratricopeptide repeat-containing proteins critical for cilia formation and function. PLoS One *10*, e0124378.

Yang, P., and Sale, W.S. (2000). Casein kinase I is anchored on axonemal doublet microtubules and regulates flagellar dynein phosphorylation and activity. J. Biol. Chem. *275*, 18905–18912.

Yelon, D., Horne, S.A., and Stainier, D.Y. (1999). Restricted expression of cardiac myosin genes reveals regulated aspects of heart tube assembly in zebrafish. Dev. Biol. *214*, 23–37.

You, Y., Richer, E.J., Huang, T., et al. (2002). Growth and differentiation of mouse tracheal epithelial cells: selection of a proliferative population. Am. J. Physiol. Lung Cell. Mol. Physiol. *283*, L1315–L1321.

Zhao, H., Zhu, L., Zhu, Y., et al. (2013). The Cep63 paralogue Deup1 enables massive de novo centriole biogenesis for vertebrate multiciliogenesis. Nat. Cell Biol. *15*, 1434–1444.

Zhu, W., Smith, J.W., and Huang, C.M. (2010). Mass spectrometry-based label-free quantitative proteomics. J. Biomed. Biotechnol. *2010*, 840518.